

Variational treatment of electron–polyatomic-molecule scattering calculations using adaptive overset grids

Loren Greenman,^{1,2,*} Robert R. Lucchese,^{1,3} and C. William McCurdy^{1,2,†}¹*Chemical Sciences Division, Lawrence Berkeley National Laboratory, Berkeley, California 94720, USA*²*Department of Chemistry, University of California, Davis, Davis, California 95616, USA*³*Department of Chemistry, Texas A&M University, College Station, Texas 77843, USA*

(Received 11 August 2017; published 27 November 2017)

The complex Kohn variational method for electron–polyatomic-molecule scattering is formulated using an overset-grid representation of the scattering wave function. The overset grid consists of a central grid and multiple dense atom-centered subgrids that allow the simultaneous spherical expansions of the wave function about multiple centers. Scattering boundary conditions are enforced by using a basis formed by the repeated application of the free-particle Green’s function and potential $\hat{G}_0^+ \hat{V}$ on the overset grid in a Born-Arnoldi solution of the working equations. The theory is shown to be equivalent to a specific Padé approximant to the T matrix and has rapid convergence properties, in both the number of numerical basis functions employed and the number of partial waves employed in the spherical expansions. The method is demonstrated in calculations on methane and CF_4 in the static-exchange approximation and compared in detail with calculations performed with the numerical Schwinger variational approach based on single-center expansions. An efficient procedure for operating with the free-particle Green’s function and exchange operators (to which no approximation is made) is also described.

DOI: [10.1103/PhysRevA.96.052706](https://doi.org/10.1103/PhysRevA.96.052706)

I. INTRODUCTION

In recent decades, three *ab initio* approaches to electron-molecule collisions and molecular photoionization have been developed and widely applied to polyatomic molecular targets: (i) the complex Kohn variational method [1–8], (ii) the Schwinger variational method [9,10], and (iii) the R -matrix method [11]. The first two of these approaches are based explicitly on variational principles and their accuracy and applicability derives from the form of the trial functions employed. The third, the R -matrix method, is an embedding approach based on dividing space into an inner region containing the molecule and an outer region in which the interactions are simpler. These approaches make different compromises in their combined numerical treatments of electronic correlation, the bound electronic states of the target molecules or ions, and the solution of the highly nonspherical electron-molecule scattering problem itself. Consequently, all three have well-recognized limitations in the size of molecules that they can treat practically. More importantly, the accuracy that can be expected of these methods when they are applied to molecules containing more than a few first-row atoms is limited by practical restrictions on the quality of the treatment of correlation and target response for larger systems, including the number and accuracy of the target electronic states that can be included.

Those limitations have their origin in the compromises made to combine the target electronic structure and correlation aspects of electron-molecule collisions with the specific method used to solve the scattering problem. In this work we demonstrate a different version of the complex Kohn approach that solves the scattering problem entirely using

adaptive grid-based methods and that substantially extends its applicability to a wider range of physical problems, including processes involving core excited states at very high energies or diffuse Rydberg-like states of polyatomic molecules. It offers a path to treat more extended systems without loss of accuracy in the solution of the scattering equations. The fundamental idea combines properties of the numerical Schwinger variational method, which has proved difficult to apply in multichannel calculations on polyatomic molecules, and the more straightforward interface with electronic-structure theory for multichannel treatments of polyatomic molecules offered by the complex Kohn approach.

Although the literature on the theory of electron-molecule collision processes and molecular photoionization is now large and well established, the results from recent experimental methods, in particular attosecond molecular photoionization [12,13] and momentum imaging measurements of dissociative electron attachment processes [14–17], are challenging the current capabilities of all existing *ab initio* methods. An example is the problem of the physics of dissociative electron attachment to DNA bases [18–20], in which the molecules are of medium size and for which the more correlated treatments currently possible for small molecules are out of the practical reach of present methods. It is becoming increasingly urgent for theory to address the highly correlated electronic continuum processes revealed in these classes of experiments when they are applied to moderate-sized polyatomic molecules.

Since it was first proposed, the Kohn variational principle [21] for scattering amplitudes has been applied using trial functions that employ a basis expansion of the scattering wave function in the interaction region combined explicitly with free-particle continuum wave functions, so that the trial function will satisfy proper scattering boundary conditions. Here we replace this form of the trial wave function with a grid-based representation making use of a version of the overset-grid approach [22–25] that is familiar in the fluid-dynamics literature. For molecules, our overset grids consist

*Present address: Department of Physics, Kansas State University, Manhattan, KS 66506, USA.

†Corresponding author: cwmccurdy@lbl.gov

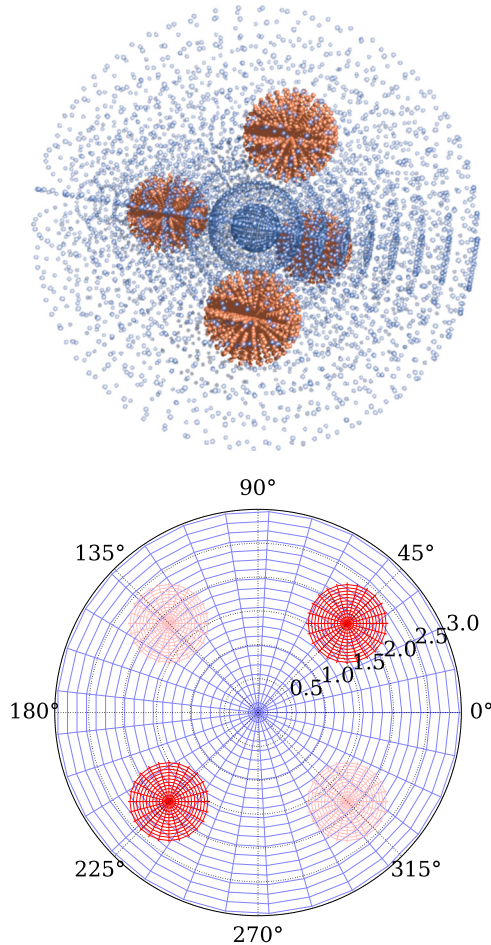


FIG. 1. Overset grids for CF_4 , in three dimensions (top panel) and in a projection (bottom panel, the darker shade is coming out of the page). These are sketches of the overset grid with relatively few points and do not represent the much denser and adaptively spaced grids used in the calculations.

of a sparse central grid located at the center of charge or an atom of interest, together with a set of dense subgrids centered on each atom. An example of a molecular overset grid is shown in Fig. 1. Wave functions are switched between grids using Becke switching functions [26]. On an overset grid, the wave function is effectively simultaneously expanded in partial waves about every nuclear center as well as about the center of the coordinate system, and this expansion converges much faster than the familiar single-center expansions that have been used, for example, in Schwinger variational calculations [9,10].

The central difficulty in applying grid methods to the Kohn variational principle is that the Kohn trial function must explicitly satisfy scattering boundary conditions and in the complex Kohn approach those must be the complex outgoing-wave boundary conditions [27,28]. To construct the trial function explicitly satisfying scattering boundary conditions using only a grid representation, we expand it in functions that are powers of $\hat{G}_0^+ \hat{V}$ operating on the incoming free-electron scattering function, where \hat{G}_0^+ and \hat{V} represent the free-particle outgoing-wave Green's function and the molecular potential, respectively. We find that this choice of basis is equivalent

to constructing a Padé approximant to the exact T matrix being approximated by the Kohn variational expression. The expansion is accomplished numerically as the basis of an iterative Arnoldi solution of the Kohn scattering equations, called Born-Arnoldi iterations here, that exhibits remarkably fast convergence, due evidently to the underlying equivalence to the construction of a Padé approximant to the solution.

In the following sections we give a complete description of the grid-based complex Kohn method and demonstrate it in calculations on small molecules. In Sec. II A we formulate the complex Kohn variational method and describe its relation to Padé approximants when implemented with the form of the trial function we are employing. We develop overset grids for molecules in Sec. II B and we describe the Born-Arnoldi procedure in Sec. II C. In Sec. II D we describe the implementation of the three-dimensional free-particle Green's function and both local and nonlocal potential operations. These are based on radial subgrids using the finite-element discrete-variable representation, which requires the application of subinterval integration weights to treat the slope discontinuity in the radial Green's functions. In Sec. III we present a series of numerical tests of the method. First, in Sec. III A, with a model problem we show that the method is invariant to using an overset grid that does not match the underlying symmetry of the potential. Then, in comparisons with electron-molecule scattering calculations using the Schwinger approach we demonstrate the advantages of the overset grids and the Born-Arnoldi procedure in Secs. III B and III C in static and static-exchange calculations on the CH_4 and CF_4 molecules.

II. THEORY AND IMPLEMENTATION

We begin by briefly describing the complex Kohn variational method, and the connection to Padé approximants when the trial function is expanded in the basis consisting of $(\hat{G}_0^+ \hat{V})^n$ operating on the incoming wave. We describe the general extension to close-coupling calculations including electron correlation and target response, to highlight some of the difficulties with applying the complex Kohn method to large molecules in its previous implementations, and then discuss how they can be overcome by using overset grids. After developing the overset grids, we present the Born-Arnoldi iteration procedure as a quickly converging method to solve the resulting system of linear equations, containing millions of variables. Finally, we illustrate the application of the necessary operations on the overset grids.

A. Complex Kohn variational method and its relation to Padé approximants

The essence of the complex Kohn variational approach can be seen easily in its formulation for a potential scattering problem. The original formulation of the variational principle by Kohn [21] made use of real-valued trial functions and reactance matrix boundary conditions. Many years later when it was reformulated with complex-valued S -matrix or T -matrix scattering boundary conditions [27,28], a complex symmetric inner product was introduced in place of the usual Hermitian inner product, thereby removing spurious singularities that appeared in numerical implementations of the original reactance matrix form. To clarify the origin of the complex symmetric

representation of the Hamiltonian that has appeared in all implementations of the complex Kohn variational method to date, we begin with the correct formulation of the complex Kohn variational principle using the conventional Hermitian inner product.

The Kohn stationary functional $T_{\mathbf{k}',\mathbf{k}}^{+S}$ of the trial functions $\psi_{\mathbf{k}}^{(+)\prime}$ and $\psi_{\mathbf{k}}^{(-)\prime}$ is

$$T_{\mathbf{k}',\mathbf{k}}^{+S} = T_{\mathbf{k}',\mathbf{k}}^{+t} + (2\pi)^{-3/2} \langle \psi_{\mathbf{k}'}^{(-)\prime} | \hat{H} - E | \psi_{\mathbf{k}}^{(+)\prime} \rangle, \quad (1)$$

where $T_{\mathbf{k}',\mathbf{k}}^{+t}$ is the asymptotic form of the trial function $\psi_{\mathbf{k}}^{(+)\prime}$, the two T matrices are labeled by asymptotic momenta, and the scattering states are $\delta_3(\mathbf{k}' - \mathbf{k})$ normalized. In this paper we will consider the case of electron-molecule scattering where only a single target electronic state is included, i.e., potential scattering from a non-spherically-symmetric nonlocal potential \hat{V} . In that case, the T matrices used in Eq. (1) have been defined such that for the exact scattering state $\psi_{\mathbf{k}}^{(+)}$, the exact T matrix is given by

$$T_{\mathbf{k}',\mathbf{k}}^+ = \langle \psi_{\mathbf{k}'}^0 | \hat{V} | \psi_{\mathbf{k}}^{(+)} \rangle, \quad (2)$$

where $\psi_{\mathbf{k}}^0$ is the unscattered plane wave. With partial-wave expansions of the scattering states of the form

$$\psi_{\mathbf{k}}^{(\pm)}(\mathbf{r}) = \sqrt{\frac{2}{\pi}} \sum_{l,m} i^l \psi_{klm}^{(\pm)}(\mathbf{r}) Y_{l,m}^*(\hat{\mathbf{k}}), \quad (3)$$

the partial-wave expansion of the T matrix is written as

$$T_{\mathbf{k}',\mathbf{k}}^+ = \sum_{l',m',l,m} (i)^{l'-l} \frac{2}{\pi} T_{k,l',m',l,m}^+ Y_{l',m'}(\hat{\mathbf{k}}') Y_{l,m}^*(\hat{\mathbf{k}}), \quad (4)$$

where

$$T_{k,l',m',l,m}^+ = \langle \psi_{kl'm'}^0 | \hat{V} | \psi_{klm}^{(+)} \rangle. \quad (5)$$

The partial-wave form of the complex Kohn variational expression is then

$$T_{k,l',m',l,m}^{+S} = T_{k,l',m',l,m}^{+t} + \langle \psi_{kl'm'}^{(-)\prime} | \hat{H} - E | \psi_{klm}^{(+)\prime} \rangle. \quad (6)$$

The traditional complex Kohn trial function has the form of the sum of contributions of a square-integrable expansion basis that describes the collision region and terms that allow it to satisfy scattering boundary conditions

$$\begin{aligned} \psi_{klm}^{(\pm)\prime} = & \sum_i c_i^{(\pm)} \varphi_i(\mathbf{r}) + \frac{1}{kr} \left[\hat{j}_l(kr) Y_{lm}(\hat{\mathbf{r}}) \right. \\ & \left. + \sum_{l',m'} T_{k,l',m',l,m}^{\pm t} \tilde{h}_l^{\pm}(kr) Y_{l',m'}(\hat{\mathbf{r}}) \right]. \end{aligned} \quad (7)$$

In Eq. (7) the functions φ_i are (usually real-valued) square-integrable functions, $\hat{j}_l(kr)$ denotes the regular Riccati-Bessel function, and $\tilde{h}_l^{\pm}(kr) \xrightarrow{r \rightarrow \infty} \hat{h}_l^{\pm}(kr)$ is a function regular at the origin that becomes the outgoing Riccati-Hankel function asymptotically. The variational parameters in this linear trial function are the coefficients $c_i^{(\pm)}$ and the T -matrix elements $T_{k,l',m',l,m}^{\pm t}$. Inserting this trial function into Eq. (6) produces the working expression, which can be written compactly in its general form for single-channel or multichannel scattering

$$\mathbf{T}^S = \mathbf{N}_{00} - \mathbf{N}_{0q} \mathbf{M}_{qq}^{-1} \mathbf{N}_{q0}. \quad (8)$$

Here the subscript 0 denotes the set of regular continuum functions $\{\hat{j}_l(kr) Y_{lm}(\hat{\mathbf{r}})/kr\}$ and the subscript q denotes the expansion basis $\{\{\varphi_i(\mathbf{r})\}, \{\tilde{h}_l^{\pm}(kr) Y_{lm}(\hat{\mathbf{r}})/kr\}\}$. The first of these matrices is the Born term and has the form

$$(\mathbf{N}_{00})_{l',m',l,m} = \left\langle \frac{\hat{j}_{l'}(kr)}{kr} Y_{l'm'}(\hat{\mathbf{r}}) \left| \hat{V} \right| \frac{\hat{j}_l(kr)}{kr} Y_{lm}(\hat{\mathbf{r}}) \right\rangle. \quad (9)$$

The matrices \mathbf{N}_{0q} and \mathbf{N}_{q0} are similarly defined. The \mathbf{M}_{qq} matrix elements are brackets of $(\hat{H} - E)$ between functions in the expansion basis. For all matrix elements in N and M , the (+) functions are used on the right-hand sides of the brackets and the (−) functions are used on the left-hand sides. This is the complex Kohn formulation that has no singularities in the matrix inverse \mathbf{M}_{qq}^{-1} at real scattering energies and it is equivalent to the S -matrix Kohn formulation of Miller and Jansen op de Haar [28]. If the basis functions on the left and right are related by the $+ \leftrightarrow -$ relationship, i.e., complex conjugation and $\vec{k} \leftrightarrow -\vec{k}$, the matrix \mathbf{M}_{qq} is complex symmetric in these approaches, unlike in the original formulation of Kohn [21], where the equivalent matrix is real symmetric.

As mentioned in Sec. I, the grid version of the Kohn variational approach must represent the continuum orbitals on the overset grid, but it must also apply the asymptotic boundary conditions in Eq. (7). We can do that by expanding ψ^t in a set of functions we construct on the grid by operating with the free-particle Green's function \hat{G}_0^+ , which here denotes the Green's function for outgoing boundary conditions $\hat{G}_0^+ \equiv (E - \hat{T} + i\epsilon)^{-1}$, where \hat{T} is the kinetic energy operator. The grid-based trial function is now

$$|\psi_{klm}^{(\pm)\prime}\rangle = |\phi_{klm}^0\rangle + \sum_{i=1}^N c_i |\phi_{i,klm}^{(\pm)}\rangle, \quad (10)$$

$$|\phi_{i,klm}^{(\pm)}\rangle \equiv (\hat{G}_0^{\pm} \hat{V})^i |\phi_{klm}^0\rangle, \quad (11)$$

with $\phi_{klm}^0 = \hat{j}_l(kr) Y_{lm}/kr$ being the incoming wave. Now all the functions in the expansion of the trial wave function, except for ϕ^0 , satisfy outgoing-wave boundary conditions ($\phi_{i,klm}^{(+)}$) or incoming-wave boundary conditions ($\phi_{i,klm}^{(-)}$) because of the asymptotic form of \hat{G}_0^{\pm} . Note that with this choice of basis functions the bra $\langle \phi_{i,klm}^{(-)} |$ satisfies

$$\langle \phi_{i,klm}^{(-)} | = \langle \phi_{klm}^0 | (\hat{V} \hat{G}_0^+)^i. \quad (12)$$

Thus, with this basis the N and M matrices can be written as

$$(\mathbf{N}_{l',m',l,m})_{i,j} = \alpha_{i+j}^{(l',m',l,m)}, \quad (13)$$

where

$$\alpha_i^{(l',m',l,m)} \equiv \langle \phi_{kl'm'}^0 | \hat{V} (\hat{G}_0^+ \hat{V})^i | \phi_{klm}^0 \rangle, \quad (14)$$

and

$$\begin{aligned} (\mathbf{M}_{l',m',l,m})_{i,j} = & \langle \phi_{i,kl'm'}^{(-)} | \hat{H} - E | \phi_{j,klm}^{(+)} \rangle \\ = & \alpha_{i+j-1}^{(l',m',l,m)} - \alpha_{i+j}^{(l',m',l,m)}, \end{aligned} \quad (15)$$

where we have used the identity $(E - \hat{T}) \hat{G}_0^{\pm} = 1$. In Sec. IID we will discuss the procedure for operating accurately and

efficiently with \hat{G}_0^\pm , but here we can make an important observation about the properties of this basis.

Nuttall [29] and Garibotti [30] observed that expressions similar to Eq. (8) could constitute Padé approximants to the equivalent exact expressions corresponding to the Schwinger variational principle, providing a particular expansion basis is used for the trial function. We have found that a similar, but not identical, result applies here. The power-series expansion of the scattered portion of the exact T matrix in the strength parameter λ has the form for elastic scattering (for simplicity) and dropping the partial-wave superscripts,

$$\begin{aligned} t &= \langle \phi_0 | \hat{V} (E - \hat{T} - \lambda \hat{V} + i\epsilon)^{-1} \hat{V} | \phi_0 \rangle \\ &= \sum_{i=0}^{\infty} \lambda^i \alpha_{i+1}. \end{aligned} \quad (16)$$

The Kohn variational approximation to Eq. (16) using the basis in Eq. (11) is the second term in Eq. (8) and for elastic scattering has the form

$$t_p^{(N)} = \vec{\alpha}^T \mathbf{M}^{-1} \vec{\alpha}, \quad (17)$$

where $\vec{\alpha} = (\alpha_1, \alpha_2, \dots, \alpha_N)$.

The key point is that Eqs. (17) and (15) have essentially the same form as Nuttall's Eqs. (28)–(30) that relate the elements of $M_{ij} = \alpha_{i+j-1} - \lambda \alpha_{i+j}$ to each other and to the elements of $\vec{\alpha}$ (differing here slightly in the definition of α_i). Using the same logic used there [29] and by Garibotti [30] we can verify that Eq. (17) produces an $[(N-1)/N]$ Padé approximant to the scattered portion of the T matrix in Eq. (16), i.e., a ratio of polynomials,

$$t_p^{(N)} = P_{N-1}(\lambda) / Q_N(\lambda) = \sum_{i=0}^{2N-1} \lambda^i \alpha_{i+1} + \mathcal{O}(\lambda^{2N}) \quad (18)$$

that reproduces the Born expansion of the scattered term in Eq. (16) to order λ^{2N-1} , but that has accelerated convergence properties. The analogous result in the case of the Schwinger expressions investigated in Refs. [29,30] and later used by Lucchese and McKoy [31] is an $[N/N]$ Padé approximant. Also note that the variational expression given in Eq. (17) is related to the $M_{2,3}^1(V S', S)$ variational expression discussed in Ref. [31] with the appropriate choice of bases.

The analysis for off-diagonal T -matrix elements is similar to that by Garibotti [30]. While we know of no general proofs concerning the rate of convergence of the Padé approximants that we effectively construct here, the connection to Padé approximants gives a strong hint as to the origins of the extraordinarily rapid rate of convergence we observe in the grid-based Kohn method demonstrated numerically in Secs. II C and III C below.

The working equations of the many-electron coupled-channel version of this theory has the form [1] of Eq. (8), but the matrices are defined in terms of the components of the many-electron trial function corresponding to incoming waves in channel Γ ,

$$\begin{aligned} \psi_{\Gamma'}^t &= \sum_{\Gamma} \mathcal{A}_{\chi_{\Gamma}}(\mathbf{r}_1 \cdots \mathbf{r}_N) F_{\Gamma}(\mathbf{r}_{N+1}) \\ &\quad + \sum_{\mu} d_{\mu}^{\Gamma'} \Theta_{\mu}(\mathbf{r}_1 \cdots \mathbf{r}_{N+1}). \end{aligned} \quad (19)$$

In previous implementations of the theory, the continuum orbitals $F_{\Gamma}(\mathbf{r}_{N+1})$ of this trial function have the form of Eq. (7) but with the T matrix now labeled additionally by channels $T_{lm,l'm'}^{\Gamma,\Gamma'}$ and incoming waves in one channel only. The correlated target state functions χ_{Γ} and the square-integrable $N+1$ electron correlation terms Θ_{μ} form the interface with electronic structure about which we will comment further below. The much larger matrix inverse portion of the working expression $\mathbf{M}_{qq}^{-1} \mathbf{N}_{q0}$ is of course found by solving linear equations, as we will do in Sec. II C in the grid implementation.

In the previous implementations of the complex Kohn variational method, a basis of atom-centered Gaussians and central Bessel functions is used to expand the trial function in Eq. (19) [5,6]. This approach has been applied successfully to a number of multichannel and single-channel electron-molecule scattering problems [1–4,8,32] and photoionization problems [7,33–35]. However, it has some drawbacks that limit its applications to larger systems. Chiefly, the exchange interaction between continuum and bound electrons is approximated. As more scattering channels are added, or more correlated target states considered and therefore more of the basis required to describe bound states, this approximation (called the separable exchange approximation since its introduction [1,2]) becomes a greater hindrance to the accurate solution of the complex Kohn equations. Additionally, at high energies, the rapid oscillation of the wave functions become more difficult to describe in this basis.

These issues have been addressed in other variational scattering methods such as the Schwinger variational method by using a single-center grid expansion of the wave function [9,10]. The Schwinger variational method has the disadvantage that describing multichannel scattering is much more difficult than in the complex Kohn variational method, which only requires a multichannel trial wave function. Furthermore, the use of single-center grid expansions limits the size of the molecules that can be considered, as we will show in Sec. III. This limitation arises because for large molecules with multiple heavy atoms, the cusps in the wave function at each nuclear position becomes more difficult to resolve as they move farther from the expansion center. It may require hundreds or thousands of angular grid points to resolve a nuclear cusp, leading to grids with tens of millions of points. This is the case even for small molecules such as CF_4 , as we will show in Sec. III. Our solution to these problems lies in the use of an overset grid.

B. Overset grid

The overset grid, pictured for CF_4 in Fig. 1, consists of a central grid (carbon centered in Fig. 1) and several smaller but denser subgrids (fluorine centered in Fig. 1). The grids we use are combinations of finite-element-method (FEM) discrete-variable-representation (DVR) grids for the radial variable in each subgrid [36–38] with Gauss-Chebyshev and Gauss-Legendre quadratures in the angular variables [39,40]. A wave function described everywhere in space can be switched onto each grid g using Becke switching functions W_g [26], commonly used in numerical density functional calculations, that smoothly switch between unity inside the

grid and zero outside it,

$$\Psi(\mathbf{r}) = \sum_g W_g(\mathbf{r})\Psi(\mathbf{r}). \quad (20)$$

The left-hand and right-hand sides of Eq. (20) are equal because the switching functions sum to unity everywhere in space,

$$\sum_g W_g(\mathbf{r}) = 1. \quad (21)$$

The right-hand side of Eq. (20) is a sum of wave functions localized on each grid,

$$\psi_g(\mathbf{r} - \mathbf{r}_{g,0}) = W_g(\mathbf{r})\Psi(\mathbf{r}), \quad (22)$$

where $\mathbf{r}_{g,0}$ is the origin of grid g . The localized functions can be expanded in local partial waves

$$\psi_g(\mathbf{r}_g) = \sum_{l,m} \frac{1}{r_g} \psi_{g,lm}(r_g) Y_{lm}(\hat{\mathbf{r}}_g), \quad (23)$$

where $\mathbf{r}_g = \mathbf{r} - \mathbf{r}_{g,0}$ and the $Y_{lm}(\hat{\mathbf{r}}_g)$ are spherical harmonics in the angular coordinates of each grid. Furthermore, there is an underlying polynomial basis of normalized Lobatto shape functions $\chi_q(r_g)$ connected to the FEM-DVR radial grids [37] so that in a direct product basis

$$X_{g,\lambda}(\mathbf{r}_g) = \chi_q(r_g) Y_{lm}(\hat{\mathbf{r}}_g), \quad (24)$$

where $\lambda = (q, l, m)$, the localized wave functions can be written as a linear combination of this basis as

$$\psi_g(\mathbf{r}_g) = \frac{1}{r_g} \mathbf{X}_g(\mathbf{r}_g) \mathbf{c}_g, \quad (25)$$

where the elements of the column vector \mathbf{c}_g are the basis expansion coefficients of the local function and \mathbf{X} is a row vector of the direct product basis defined in Eq. (24),

$$\mathbf{X}_g(\mathbf{r}_g) = [X_{g,1}(\mathbf{r}_g), X_{g,2}(\mathbf{r}_g), \dots, X_{g,N}(\mathbf{r}_g)]. \quad (26)$$

Our choice of the angular quadratures allow an efficient transformation between the grid and spherical harmonic representations [40].

We will discuss in detail the operations necessary for the Born-Arnoldi scheme in Sec. II D, but here we consider how operators are represented in the overset-grid approach. A three-dimensional function $\Psi(\mathbf{r})$ is defined by its value on the grid points \mathbf{r}_g on all grids labeled by the different values of g . For a local operator $\hat{O} = \hat{O}(\mathbf{r})$, we have

$$(\hat{O}\Psi)(\mathbf{r}) = \hat{O}(\mathbf{r})\Psi(\mathbf{r}). \quad (27)$$

For nonlocal operators, e.g., exchange operators and Green's functions, \hat{O} operating on a set of local function $\hat{O}\psi_g$ can be calculated using \mathbf{O}_g , which is the matrix representation of the operator \hat{O} in the direct product basis defined in Eq. (24), so that

$$(\hat{O}\psi_g)(\mathbf{r}_g) = \frac{1}{r_g} \mathbf{X}(\mathbf{r}_g) \mathbf{O}_g \mathbf{c}_g, \quad (28)$$

For example, \mathbf{O}_g for a local potential is its matrix representation in the product basis, diagonal in radial discrete-variable-representation (DVR) points. We describe the construction of

the \mathbf{O}_g for the exchange operator and free-particle Green's function in Sec. II D below.

The off-grid contributions must be calculated by interpolation or extrapolation. The FEM-DVR and spherical harmonic expansions lend themselves to interpolating accurately due to the underlying orthogonal polynomial bases. If the maximum radius of the grid in region g is $r_{g,x}$, then the off-grid points are obtained from a matrix transform [41]

$$\begin{aligned} & (\hat{O}\psi_g)(\mathbf{r} - \mathbf{r}_{g,0}) \\ &= \begin{cases} \frac{1}{|\mathbf{r} - \mathbf{r}_{g,0}|} \mathbf{X}_g(\mathbf{r} - \mathbf{r}_{g,0}) \mathbf{O}_g \mathbf{c}_g & \text{for } |\mathbf{r} - \mathbf{r}_{g,0}| < r_{g,x} \\ \mathbf{Z}_g(\mathbf{r} - \mathbf{r}_{g,0}) \mathbf{O}_g^a \mathbf{c}_g & \text{otherwise,} \end{cases} \end{aligned} \quad (29)$$

where \mathbf{Z}_g is a row vector of the asymptotic partial-wave expansion terms of the operator \hat{O} outside the grid g , whose length is the number of spherical harmonics used in the direct product basis. Note that \mathbf{O}_g^a is a rectangular matrix with the number of rows being the number of spherical harmonics used in the direct product basis, i.e., the length of the row vector \mathbf{Z}_g , and with the number of columns being the size of the direct product basis, i.e., the length of the column vector \mathbf{c}_g . For example, in the case of $1/r_{12}$ in the exchange operator, the asymptotic forms for a system with no symmetry would be

$$\begin{aligned} \mathbf{Z}_g(\mathbf{r}_g) = & \left[\frac{1}{r_g} Y_{00}(\hat{\mathbf{r}}_g), \frac{1}{r_g^2} Y_{11}(\hat{\mathbf{r}}_g), \frac{1}{r_g^2} Y_{10}(\hat{\mathbf{r}}_g), \frac{1}{r_g^2} Y_{1,-1}(\hat{\mathbf{r}}_g), \right. \\ & \left. \times \frac{1}{r_g^3} Y_{2,-2}(\hat{\mathbf{r}}_g), \frac{1}{r_g^3} Y_{2,-1}(\hat{\mathbf{r}}_g), \dots \right], \end{aligned} \quad (30)$$

where the number of elements is just given by the number of spherical harmonics used in the direct-product basis. In that case the matrix \mathbf{O}_g^a would be the implementation of the integral in Eq. (50) for points outside the region g . The operation on the total wave function can then be determined by

$$(\hat{O}\Psi)(\mathbf{r}) = \sum_g (\hat{O}\psi_g)(\mathbf{r} - \mathbf{r}_{g,0}). \quad (31)$$

In the single-channel calculations that we present here the matrix inverse portion of the complex Kohn working expression in Eqs. (8) and (9) is equivalent to the solution of a driven equation

$$(E - \hat{H})|\Psi^{\text{scat}}\rangle = \hat{V} \left| \frac{\hat{j}_l(kr)}{kr} Y_{lm}(\hat{\mathbf{r}}) \right\rangle \quad (32)$$

of the Schrödinger equation, which when expressed directly on the overset grid becomes a set of linear equations for the quantity $\Psi^{\text{scat}} = \mathbf{M}_{qq}^{-1} \mathbf{N}_{q0}$. The coordinate \mathbf{r} in Eq. (32) is defined in the central grid of the overset grid. Three problems arise in solving the complex Kohn driven equations (32) on the grid: (i) Outgoing-wave scattering boundary conditions must be imposed on the solution, (ii) the linear equations on the overset grids can contain on the order of millions of variables, and (iii) interpolating the derivatives required by the kinetic energy operator in \hat{H} between grids as required in Eq. (31) is numerically problematic due to the oscillations of the DVR of the derivative operator between grid points. The use of the Born-Arnoldi iterative basis defined in Eq. (11) and the Kohn

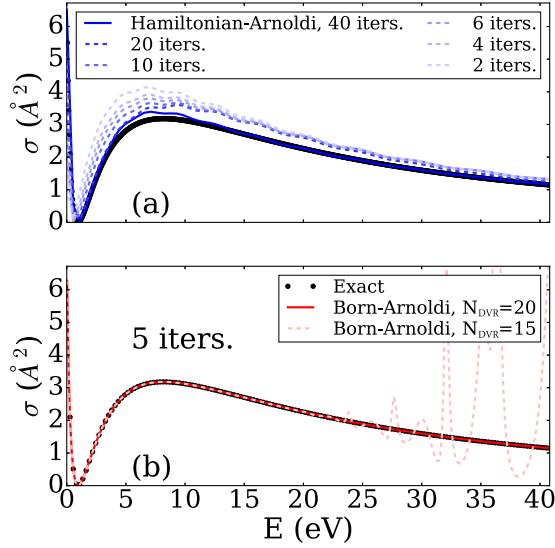


FIG. 2. Partial scattering cross sections for s waves for the spherical potential $V = -3e^{-r}$. (a) Hamiltonian-Arnoldi iterates of $E - \hat{H}$ converge slowly to the exact result. (b) Born-Arnoldi iterates converge at only five iterations, including the case where the order of the DVR in each finite element is increased to represent the scattered wave at higher energies.

variational expression given in Eq. (8) will be seen to overcome these problems.

C. Born-Arnoldi iteration

By building a basis to solve Eq. (32) using the Born series $(\hat{G}_0^+ \hat{V})^n \hat{Y}_l Y_{lm}/kr$, we have a physically motivated basis that automatically satisfies the outgoing-wave scattering and that is quickly convergent, evidently because of its equivalence to a Padé approximant. Additionally, as we will show in this section, this basis eliminates the need for interpolating the action of the kinetic energy operator $\hat{T}\Psi$, significantly reducing the numerical error in the overset-grid representation.

We aim to solve the driven equation of the complex Kohn variational method, Eq. (32) with $E = k^2/2$, in order to construct the T -matrix elements $T_{lm,l'm'}$. To compare to a more standard Arnoldi iterative approach, we solved those equations with a basis of Arnoldi iterates of $E - \hat{H}$ operating repeatedly on the right-hand side of Eq. (32), applied a cutoff to prevent the results from reaching the end of the grid, and then added a single function on the grid that satisfies outgoing-wave boundary conditions in each partial wave. This procedure is analogous to the construction of the traditional Kohn trial function in Eq. (7). In Fig. 2 we demonstrate that this procedure, which is labeled “Hamiltonian-Arnoldi,” converges quite slowly. We have also found that this procedure converges even more slowly at higher energies.

The issues of slow Arnoldi convergence and application of the proper boundary conditions are both addressed by using iterates of the Born series $(\hat{G}_0^+ \hat{V})^n \hat{Y}_l Y_{lm}/kr$, beginning with $n = 1$. As discussed Sec. II A, using this basis is equivalent to constructing an $[(N - 1)/N]$ Padé approximate to the elements of the scattered portion of the T matrix. In addition, the application of the outgoing free-particle Green’s

function \hat{G}_0^+ ensures that every member of the basis satisfies outgoing-wave boundary conditions. The zeroth iterate is set to $\phi_0 = \hat{Y}_l Y_{lm}/kr$ [ϕ_0 does not have the proper boundary conditions and is not used to solve Eq. (32)]. Subsequent orthogonal iterates are generated as

$$\tilde{\phi}_{k+1}^+ = \hat{G}_0^+ \hat{V} \phi_k^+, \quad (33)$$

$$\bar{\phi}_{k+1}^+ = \tilde{\phi}_{k+1}^+ - (\tilde{\phi}_{k+1}^+, \phi_j^+) \phi_j^+ \forall j \leq k, \quad (34)$$

$$\phi_{k+1}^+ = \bar{\phi}_{k+1}^+ / (\bar{\phi}_{k+1}^+, \bar{\phi}_{k+1}^+)^{1/2}. \quad (35)$$

The products (ϕ_1^+, ϕ_2^+) in Eqs. (33)–(35) are symmetric products rather than Hermitian inner products,

$$(\phi_1^+, \phi_2^+) = \int \phi_1^+ \phi_2^+ d^3r. \quad (36)$$

Note that this form of the inner product for functions expanded in real-valued symmetry-adapted harmonics, as is done in the actual calculations, is equivalent to the Hermitian inner product with the $(-)$ form of the functions on the left side and the $(+)$ form on the right, i.e., $\langle \phi_1^- | \phi_2^+ \rangle$.

The use of the Born iterates also eliminates the necessity in the application of $E - \hat{H}$ to operate numerically with the kinetic energy operator. The matrix elements of $E - \hat{H}$ in this basis are easily constructed using the fact that \hat{G}_0^+ is the Green’s function of $E - \hat{T}$. All the terms in this basis, contributing to matrix elements $\langle \phi_j^- | E - \hat{H} | \phi_k^+ \rangle$ in the representation of Eq. (32), involve the operation

$$\begin{aligned} (E - \hat{H}) \hat{G}_0^+ \hat{V} \phi^+ &= (E - \hat{T} - \hat{V}) \hat{G}_0^+ \hat{V} \phi^+ \\ &= (\hat{T} - \hat{V} \hat{G}_0^+) \hat{V} \phi^+ \\ &= \hat{V} (\phi^+ - \hat{G}_0^+ \hat{V} \phi^+). \end{aligned} \quad (37)$$

Since the quantities ϕ^+ and $\hat{G}_0^+ \hat{V} \phi^+$ are calculated for all ϕ^+ functions in the basis, they can be simply combined to construct the result of $E - \hat{H}$ operating on any ϕ_k^+ . The calculation of the matrix element $\langle \phi_j^- | E - \hat{H} | \phi_k^+ \rangle$ is completed by using the quadratures and switching functions for each grid.

D. Operating with \hat{G}_0^+ and \hat{V}

To complete the algorithm for solving the complex Kohn equations we require efficient ways with which to operate with \hat{G}_0^+ and the potential on the overset grid. The potential energy operator in each channel and the coupling potentials between channels are, in general, combinations of direct operators and nonlocal exchange operators. The essential observation is that since both the free-particle Green’s function \hat{G}_0^+ and the potential energy of electron repulsion $1/|\mathbf{r} - \mathbf{r}'|$ are translationally invariant, we can transform to the single-center expansion around the center of each subgrid when operating on that grid. Exploiting that translational invariance efficiently requires the fast transformation between quadrature points and the spherical harmonic expansion developed earlier [40] and this is the central idea that allows the overset-grid method to effectively expand the wave function around all the nuclear centers and the center of the central grid simultaneously.

We use the integral form of the free-electron Green's function \hat{G}_0^+ , operating in the partial-wave basis of Eq. (23),

$$\hat{G}_0^+ \psi_g(\mathbf{r}_g) = \sum_{l,m} -\frac{2}{kr_g} Y_{lm}(\hat{\mathbf{r}}_g) \times \int \hat{j}_l(kr_{<,g}) \hat{h}_l^+(kr_{>,g}) \psi_{g,lm}(r'_g) dr'_g. \quad (38)$$

In Eq. (38), \hat{h}_l^+ is the outgoing Riccati-Bessel function, the arguments of \hat{j}_l and \hat{h}_l^+ depend on whether $r_g < r'_g$, and \hat{G}_0^+ is diagonal in the partial-wave basis. The local wave functions on each grid are expanded in terms of the FEM-DVR local radial basis functions $\chi_q(r)$ and the wave function evaluated at Gauss-Lobatto quadrature points r_q ,

$$\psi_{g,lm}(r_g) = \sum_q \psi_{g,lm}(r_q) \chi_q(r_g). \quad (39)$$

At the FEM-DVR element boundaries R_b , the integrals in Eq. (38) can be performed using the Gauss-Lobatto quadrature with weights w_q ,

$$(\hat{G}_0^+ \psi_{g,lm})(R_b) = -\frac{2}{k} \sum_q w_q \hat{j}_l(kr_{<}) \hat{h}_l^+(kr_{>}) \psi_{g,lm}(r_q), \quad (40)$$

where $r_{<}$ and $r_{>}$ are the minimum and maximum, respectively, of R_b and r_q .

More care must be taken [42] when evaluating the integral in Eq. (38), $(\hat{G}_0^+ \psi_{g,lm})(r_i)$, at quadrature points r_i within an FEM-DVR element because of the slope discontinuity at $r = r'$. Naively, the sum in Eq. (40) might be cut off at $q = r_i$. This approximation corresponds, however, to integrating a function across the entire boundary region that is represented by a polynomial whose values at the quadrature points drop suddenly from the integrand values of Eq. (38) before r_i to zero following r_i . The resulting polynomial approximation is highly oscillatory and only on very dense FEM-DVR grids does it represent the integrand accurately.

A far better choice for evaluating Eq. (38) at the interior points is obtained by integrating the basis functions $\chi_q(r)$ of Eq. (39), which are the cardinal functions of the DVR representation, to obtain integration weights $\Omega_{q',q}$ adapted to integrating over the subintervals ending at the quadrature point $r_{q'}$. For the example of the finite element beginning at 0 and ending at R_b we define the adapted weights

$$\Omega_{q',q}^< = \int_0^{r_{q'}} \chi_q(r) dr, \quad (41)$$

$$\Omega_{q',q}^> = \int_{r_{q'}}^{R_b} \chi_q(r) dr. \quad (42)$$

These weights can be calculated exactly using the same order DVR that defines the cardinal functions $\chi_q(r)$ by rescaling the integration variable in, e.g., Eq. (41),

$$\Omega_{q',q}^< = \int_0^{R_b} \chi_q\left(\frac{r_{q'}}{R_b} r\right) \frac{r_{q'}}{R_b} dr \quad (43)$$

and evaluating the basis functions χ_q at the rescaled points. The Green's-function result at the interior points r_i is therefore

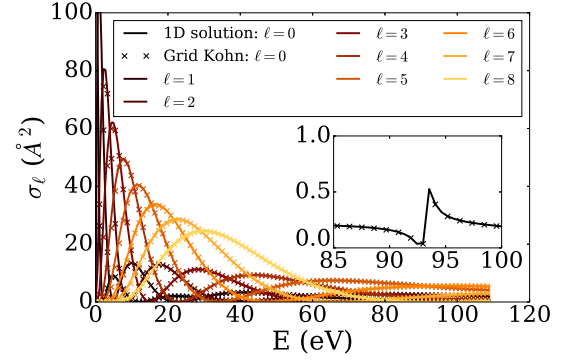


FIG. 3. Cross sections σ_l in each angular momentum channel l are given for the Noro-Taylor potential $V = \frac{15}{2} r^2 e^{-r}$. The solid lines are numerically exact results calculated using exterior complex scaling and the crosses are the results calculated using the complex Kohn method on the CH₄ overset grid. Even though the potential is peaked at the subgrid locations, the grid-based Kohn method is accurate even in the difficult region of the narrow s -wave resonance (inset).

given as a matrix-vector product of the adapted weights and the wave functions evaluated across the entire element

$$(\hat{G}_0^+ \psi_{g,lm})(r_i) = \hat{h}_l^+(kr_i) \sum_q \Omega_{i,q}^< \hat{j}_l(kr_q) \psi_{g,lm}(r_q) + \hat{j}_l(kr_i) \sum_q \Omega_{i,q}^> \hat{h}_l^+(kr_q) \psi_{g,lm}(r_q), \quad (44)$$

producing a significantly more accurate result than truncating the quadrature at the interior point.

After calculating the on-grid result of the Green's function, we must interpolate it to obtain the off-grid result

$$(\hat{G}_0^+ \psi_g)(\mathbf{r}_{g'}) = -\frac{2}{kr_g[\mathbf{r}_{g'}]} \sum_{q,lm} (\hat{G}_0^+ \psi_{g,lm})(r_q) \chi_q(r_g[\mathbf{r}_{g'}]) Y_{lm}(\hat{\mathbf{r}}_g[\mathbf{r}_{g'}]). \quad (45)$$

The interpolants here are again calculated using the cardinal functions for the radial variables and spherical harmonics for the angular variables.

We must also calculate the operation of the potential \hat{V} . For local potentials, e.g., model potentials for which results are shown in Figs. 2 and 3, or the Coulomb potential, we calculate the potential directly on the coordinates of each grid,

$$(\hat{V} \psi_g)(\mathbf{r}_g) = V(\mathbf{r}_g) \psi_g(\mathbf{r}_g). \quad (46)$$

The nuclear potentials for each atom are such local potentials, but they are singular at the origin of each subgrid, behaving as $-Z/r$. The radial functions $\psi_{g,lm}(r)$ in Eqs. (39) and (40) are r times the complete radial function and tend to zero at the grid origins. We therefore use L'Hôpital's rule to determine $\hat{V} \psi_g$ at the grid origins,

$$(\hat{V}_{\text{nuc}} \psi_{g,lm})(r_g \neq 0) = -\frac{Z}{r_g} \psi_{g,lm}(r_g), \quad (47)$$

$$(\hat{V}_{\text{nuc}} \psi_{g,lm})(0) = -Z \left. \frac{\partial \psi_{g,lm}}{\partial r_g} \right|_{r_g=0}. \quad (48)$$

Equation (48) is only evaluated for the nucleus at the center of the grid g and the derivative $\chi'_q(0)$ is evaluated using the analytic derivative of the FEM-DVR basis functions that include the cardinal function that is nonzero at the origin.

The static Coulomb potential due to an electron in an occupied orbital φ is a nonsingular local potential

$$(\hat{J}\{\varphi\}\psi_g)(\mathbf{r}_g) = \int \frac{|\varphi(\mathbf{r}')|^2}{|\mathbf{r}' - (\mathbf{r}_g + \mathbf{r}_{g,0})|} \psi_g(\mathbf{r}_g) d^3r'. \quad (49)$$

The molecular orbitals from, for instance, a Hartree-Fock calculation in a Gaussian basis can be used to provide a static Coulomb potential. In this case, the integrals of Eq. (49) evaluated at each grid point on the overset grid are Gaussian nuclear electrostatic potential integrals. These can be computed by standard Gaussian integral libraries in widely available quantum chemistry software, and we use the LIBINT integral library [43] to compute them.

The exchange potential due to an electron in an orbital φ is an example of a nonlocal potential and we calculate the exchange potential using a mechanism similar to the Green's-function operation. The $1/r_{12}$ integrals of the exchange operator can be calculated in the partial-wave basis using the spherical multipole expansion of the Coulomb interaction

$$\begin{aligned} &(\hat{K}\{\varphi\}\psi_g)(\mathbf{r}_g) \\ &= \varphi(\mathbf{r}_g) \sum_{l,m} \frac{4\pi}{2l+1} Y_{lm}(\hat{\mathbf{r}}_g) \int \frac{r'^l_{<,g}}{r'^{l+1}_{>,g}} (\varphi\psi_g)_{lm}(r'_g) dr'_g, \end{aligned} \quad (50)$$

where $(\varphi\psi_g)_{lm}$ has an overall multiplicative factor of r_g^2 coming from the product of two partial-wave radial functions. Equation (50) is analogous to Eq. (38) with $4\pi/(2l+1)$ replacing $-2/k$, $r'^l_{<,g}$ replacing $\hat{j}_l(kr_{<,g})$, and $r'^{-l+1}_{>,g}$ replacing $\hat{h}_l^+(kr_{>,g})$. The action of any exchange interaction operator is evaluated in the same manner as the Green's function, with these constants and functions substituted.

We thus exploit the translational invariance of the underlying operator $1/r_{12}$ to allow the use of a separate single-center expansion about the origin of each subgrid. The combination of these local expansions and the adapted weights for integrations like that in Eq. (40) produces an accurate representation on the overset grid of the action of both \hat{G}_0^+ and the local and exchange portions of \hat{V} .

III. NUMERICAL RESULTS

We have implemented the complex Kohn variational method on overset grids using the computational infrastructure of the electron-molecule scattering code suite ePolyScat [40,44] originally developed for calculations using the Schwinger approach. This implementation allows interfacing with a number of quantum chemistry code suites including MOLPRO [45,46] and GAUSSIAN [47] to provide molecular orbitals from Hartree-Fock calculations and other target electronic-structure information. Below we discuss the application to both model potentials and to single-channel molecular static (Coulomb operators only) and static-exchange approximations.

A. One-dimensional spherical potential

An initial test of the overset-grid method in three dimensions was to solve a spherical potential scattering problem, scattering from the Noro-Taylor potential [48], with a nonspherically symmetric overset grid. The Noro-Taylor potential, in atomic units,

$$V(r) = \frac{15}{2} r^2 e^{-r} \quad (51)$$

is 0 at $r = 0$, rises to a peak of 110.48 eV at $r = 2$ bohrs, which is approximately the C—H bond distance in methane, and falls to about 0.93 eV at $r = 10$ bohrs. In s -wave scattering this potential supports a narrow resonance near a scattering energy of 95.2 eV. We used an overset grid based on the tetrahedral geometry of CH₄. Thus we had a central grid centered at the origin coinciding with the location of the C atom of CH₄ and four subgrids located away from the origin centered at the location of the H atoms in CH₄. Thus the grid for this problem was qualitatively the same as that depicted in Fig. 1. We observed that the overset grid does not modify the scattering amplitudes of the Noro-Taylor potential for any partial wave, nor does it suffer from any apparent numerical pathologies associated with the obvious linear dependence of the underlying spectral basis in the overlapping subgrids and central grid. That result is shown in Fig. 3.

B. CH₄ static Coulomb and static-exchange potentials

The central difficulty in the application of single-center expansions to the solution of scattering problems is resolving the nuclear potentials of atoms not at the center of the coordinate system, which can require values of ℓ in the hundreds even for relatively small systems. This problem of course becomes more severe as heavy atoms are added far from the expansion center, as we will find in Sec. III C. In the examples we explore here, we will compare the grid-based complex Kohn approach with the numerical Schwinger method, which relies on a single-center expansion and outward radial integration beyond the range of the exchange potential, seeking convergence of the integral cross section in all cases to within 0.01 \AA^2 .

We begin by exploring the cross sections for scattering from the static Coulomb potential of CH₄, calculated using a STO-3G basis [49,50]. We used the GAUSSIAN package [47] to calculate the Hartree-Fock molecular orbitals. In Fig. 4 we show the cross sections for the CH₄ static potential for both the single-center expanded Schwinger variational method and the complex Kohn method on the overset grid. The single-center expansion is converged using partial waves up to $\ell = 40$ and the grid-based Kohn method reproduces that result using only $\ell \leq 15$.

We show the analogous calculation of the cross sections for the CH₄ static-exchange potential in Fig. 5. The potentials due to CH₄ are mostly spherical due to the small perturbations of the hydrogen atoms, so both the single-center Schwinger variational method and the overset-grid complex Kohn method converge quickly. For the Schwinger method, expanding in partial waves with $\ell \leq 20$ and $\ell \leq 10$ gives a similar result, while $\ell \leq 5$ and $\ell \leq 3$ depart considerably from the converged values. The overset-grid complex Kohn method

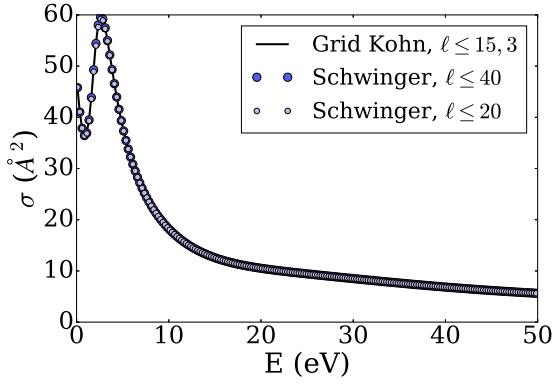


FIG. 4. Integral cross section for electron-molecule scattering from the static potential of CH_4 as a function of energy: The single-center expanded Schwinger variational method result is shown with partial waves up to $\ell = 40$ (larger dark blue circles) and $\ell = 20$ (smaller light blue circles). Overset-grid complex Kohn method cross sections are shown as a solid black line. Partial waves only up to $\ell = 15$ on the central grid and $\ell = 3$ on the subgrid are required for similar convergence in the complex Kohn method.

converges more rapidly, converging at $\ell \leq 5$ until an energy of 50–60 eV and completely converging with $\ell \leq 15$. While the CH_4 calculations test that the method is viable, a more nonspherical potential is necessary to show that it is a significant improvement over single-center methods.

C. CF_4 static Coulomb and static-exchange potentials

CF_4 presents a more serious challenge for single-center expansion methods because of the $Z = 9$ F atoms located 1.315 Å from the carbon center. While for CH_4 , 1681 partial waves with $\ell \leq 40$ were required to resolve the static Coulomb potential, for CF_4 the number of partial waves

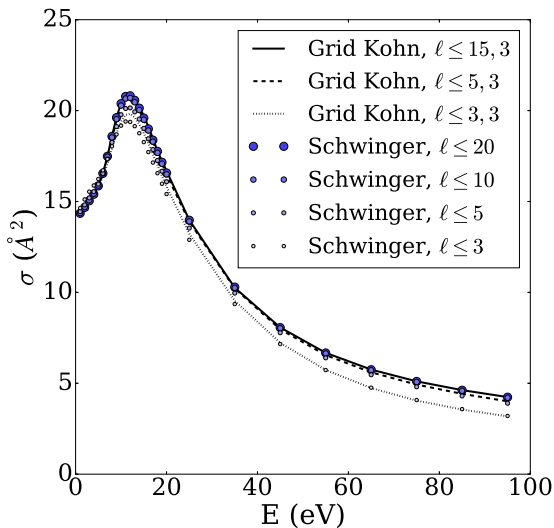


FIG. 5. Total cross sections σ for electron-molecule scattering from the static-exchange potential of CH_4 are given as a function of energy. We make a comparison between the single-center Schwinger variational method (blue circles) from $\ell \leq 3$ (smallest) to $\ell \leq 20$ (largest) and the overset-grid complex Kohn method for $\ell \leq 3$ (dotted line), $\ell \leq 5$ (dashed line), and $\ell \leq 15$ (solid line) on the central grid and $\ell \leq 3$ on the subgrids.

TABLE I. Convergence of the Born-Arnoldi iterations for electron- CH_4 and - CF_4 scattering for different sizes of grids. Here $\ell_{\text{max}} = \ell_{\text{cg}}/\ell_{\text{sg}}$ denotes the ℓ_{cg} maximum angular momentum on the central grid and ℓ_{sg} on subgrids. All cases refer to the T_2 symmetry component in the static-exchange approximation at 6 eV.

Molecule	ℓ_{max}	Grid points	Born-Arnoldi iterations
CH_4	15/3	1 105 920	9
CH_4	5/3	366 720	11
CF_4	15/3	1 228 800	24
CF_4	35/3	2 352 000	22

required increases dramatically. For $\ell \leq 100$ (10 201 partial waves), the change in many calculated cross sections slowed to about 0.1 \AA^2 per increase of ℓ_{max} by 20. However, as we will show, complete convergence is not reached even by $\ell_{\text{max}} = 200$ (40 401 partial waves). In contrast, the complex Kohn method on the overset grid converges to 0.01 \AA^2 between $\ell = 35$ and $\ell = 45$. Those values of ℓ correspond to 1296–2116 partial waves on the central grid and 16 partial waves on each subgrid.

The total number of grid points on the union of the overset grids is therefore in the millions for the complex Kohn calculations, which however is much smaller than the corresponding single center grid largely because of the more rapid convergence with partial waves in the central and subgrids. Nonetheless, as demonstrated in Table I, the number of Born-Arnoldi iterations remains less than about 25 even when the number of grid points is doubled. The number of iterations is effectively the number of basis functions in the expansion of the trial wave function in Eq. (11). At resonances slightly more iterations can be required, but we observe similar convergence properties in the Born-Arnoldi iterations in all the calculations reported in Sec. III. The origin of this remarkable numerical behavior is evidently the underlying connection to an $[(N - 1)/N]$ Padé approximant to the scattered part of the T matrix discussed in Sec. II A.

In Fig. 6 we show the cross sections for the CF_4 static potential, using the single-center Schwinger variational method and the complex Kohn method on the overset grid. From $\ell = 60$ to $\ell = 120$, there is a significant change in the results obtained using the single-center expansion. Resolving the static potential is particularly difficult for the single-center expansion as the slow convergence of the result shows. The overset-grid method, on the other hand, is converged at the small number of partial waves given by $\ell = 25$ in the central grid and $\ell = 3$ in the subgrid. By expanding the nuclear potentials in the spherical polar coordinates of their proper centers, we dramatically reduce the computational effort.

In Fig. 7 we compare the same methods for the static-exchange potential of CF_4 at the HF/6-31G* [51–53] level of theory. The static-exchange potential models the physical electron-molecule scattering potential of CF_4 for elastic scattering, although electron correlation and target response effects are neglected. The differences between the cross sections calculated using the overset-grid Kohn method with $\ell_{\text{max}} = 3$ in the subgrids and with $\ell_{\text{max}} = 15, 25,$ and 35 in the central grid are small, especially outside the region of the resonance and except at very low energies. In the region of the resonances

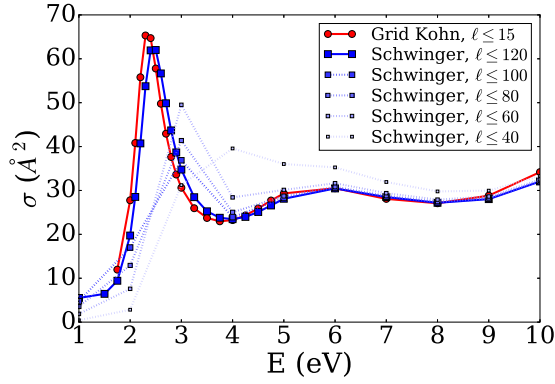


FIG. 6. Comparison of the cross sections for the static Coulomb potential of CF_4 . The complex Kohn method on the overset grid (red circles, solid line) is shown with $\ell_{\text{max}} = 15$ in the central grid and $\ell_{\text{max}} = 3$ in the subgrids. Results with the single-center expanded Schwinger variational method at various ℓ_{max} are shown (fading purple squares, dotted lines), including an approximately converged reference line at $\ell_{\text{max}} = 120$ (blue square, solid line). The single-center results converge slowly with the number of partial waves, while the overset-grid results are largely converged with very few partial waves.

(one T_2 resonance and about 10.0 eV and one A_1 resonance at about 11.5 eV), the cross section calculated at $\ell = 15$ is slightly low. However, the shape of the resonance features is close to the converged shape even with the lowest number of partial waves shown, which is not the case for the unconverged single-center expansion result from the Schwinger calculations.

At energies below 10 eV in Fig. 7, the single-center expansion cross sections converge very slowly. At lower energies, the effects of the potentials near the nuclei are becoming increasingly important, as is evidenced by the fact that this is the most difficult region of the cross section to converge in the single-center expansion. In Table II we choose $E = 6$ eV

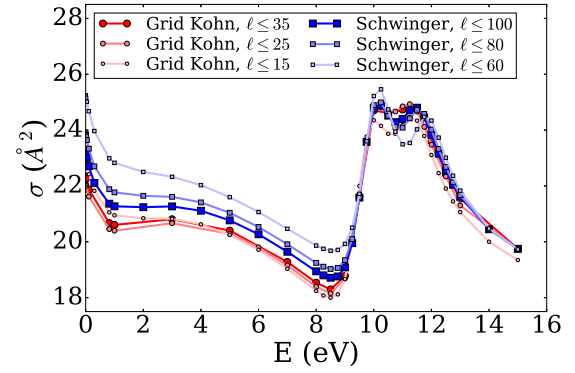


FIG. 7. Comparison of the cross sections for the static-exchange potential of CF_4 . The grid Kohn method (red circles, various fading) are given for subgrids with $\ell = 3$ and central grid with $\ell = 15, 25,$ and 35 . The nonresonance features match for all three, while the resonance features converge at $\ell = 25$. The single-center expanded Schwinger method (blue squares, various fading) is shown for $\ell = 60, 80,$ and 100 for which some of the features are not converged even for maximum $\ell = 200$.

to explore the convergence of the single-center expansion Schwinger method and compare it to the convergence of the overset-grid complex Kohn method. Although no exact result is available, the rates of convergence of the two methods can be judged at least approximately from the changes as ℓ_{max} is incremented which are shown in the table. By that measure, the total cross section from the overset-grid Kohn method is converged to 0.01 \AA^2 by $\ell = 35$ in the central grid and increasing the subgrid angular grid from $\ell = 3$ to $\ell = 6$ has no effect. The A_1 and T_2 components of the cross section converge to 0.0017 and 0.0030 \AA^2 , respectively. In contrast, the single-center expansion results converge to only 0.02 \AA^2 at $\ell = 200$. To demonstrate conclusively that these methods are converging to the same result to two digits

TABLE II. Convergence of the integral cross section and its dominant symmetry components at $E = 6$ eV for CF_4 in the static-exchange approximation (in units of \AA^2 , with differences in parentheses). Schwinger variational cross sections using a single-center expansion are given from $\ell = 60$ to $\ell = 200$. Overset-grid complex Kohn cross sections are given for the central grid $\ell = 15$ to $\ell = 45$, by which an effectively converged result is obtained. For the overset grids ℓ_{max} is denoted as $\ell_{\text{cg}}/\ell_{\text{sg}}$ as in Table I.

ℓ_{max}	A_1		E		T_2		Total	
Schwinger variational method, single-center expansion								
60	7.9166		0.2322		4.2152		21.0662	
80	7.8290	(-0.0876)	0.2315	(-0.0007)	4.0662	(-0.1491)	20.5299	(-0.5363)
100	7.7752	(-0.0538)	0.2313	(-0.0002)	3.9974	(-0.0688)	20.2694	(-0.2606)
120	7.7442	(-0.0309)	0.2313	(-0.0001)	3.9623	(-0.0351)	20.1330	(-0.1364)
140	7.7259	(-0.0184)	0.2312	(-0.0000)	3.9426	(-0.0197)	20.0556	(-0.0774)
160	7.7144	(-0.0115)	0.2312	(-0.0001)	3.9306	(-0.0120)	20.0081	(-0.0475)
180	7.7075	(-0.0069)	0.2312	(0.0001)	3.9238	(-0.0068)	19.9807	(-0.0274)
200	7.7027	(-0.0048)	0.2312	(-0.0000)	3.9189	(-0.0048)	19.9613	(-0.0193)
Complex Kohn variational method, overset-grid expansion								
15/3	7.7536		0.2107		3.8348		19.7149	
25/3	7.6605	(-0.0931)	0.2309	(0.0202)	3.8795	(0.0448)	19.8001	(0.0853)
35/3	7.6907	(0.0302)	0.2314	(0.0005)	3.9083	(0.0288)	19.9179	(0.1178)
35/6	7.6907	(-0.0000)	0.2314	(-0.0000)	3.9083	(-0.0000)	19.9178	(-0.0000)
45/3	7.6890	(-0.0017)	0.2312	(-0.0002)	3.9053	(-0.0030)	19.9066	(-0.0112)

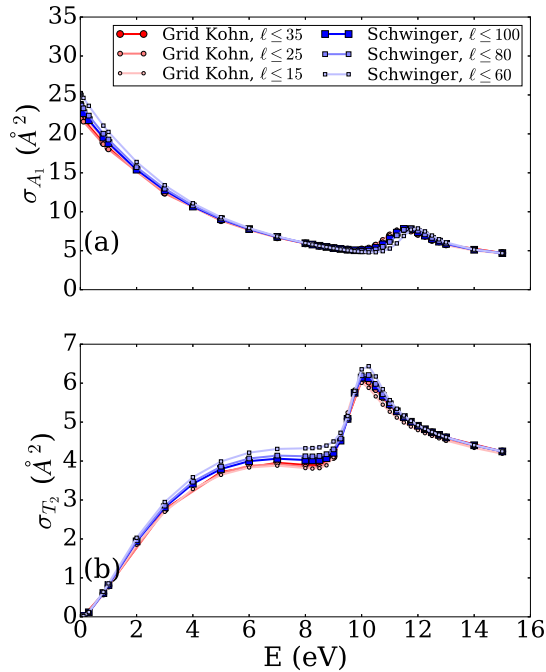


FIG. 8. The (a) A_1 and (b) T_2 components of the static-exchange cross section of CF_4 . The grid Kohn method cross sections (red circles, various fading) and single-center expanded Schwinger method cross sections (blue squares, various fading) are compared.

beyond the decimal would require Schwinger calculations substantially beyond $\ell = 200$, which rapidly become computationally prohibitive.

We have also examined the symmetry components of the cross sections as a function of energy, shown in Fig. 8. Here we can see in more detail what is happening as the resonance regions converge. For the single-center expanded Schwinger method, the A_1 resonance is moving to lower energies as it converges [10]. The overset-grid Kohn method, in comparison, converges its prediction of the A_1 resonance energy closely by $\ell = 15$. At very low energies, the Schwinger method also converges slowly compared to the grid Kohn method. The

TABLE III. Convergence of integral cross sections for the static-exchange potential of CF_4 using the Schwinger method with single-center expansion and the overset-grid complex Kohn method for four points of interest: the A_1 components at 0.01 and 0.1 eV, the A_1 resonance at 11.5 eV, and the T_2 resonance at 10.0 eV.

ℓ_{\max}	A_1				T_2			
	0.01 eV		0.1 eV		11.5 eV		10.0 eV	
Schwinger variational method, single-center expansion								
60	25.1782		24.6777		6.8941		6.3549	
120	22.8114	(-2.3667)	22.3826	(-2.2951)	7.8005	(0.9064)	6.1151	(-0.2398)
140	22.6240	(-0.1874)	22.2007	(-0.1819)	7.7918	(-0.0087)	6.1006	(-0.0145)
160	22.5088	(-0.1152)	22.0889	(-0.1118)	7.7837	(-0.0081)	6.0924	(-0.0082)
180	22.4438	(-0.0650)	22.0256	(-0.0633)	7.7766	(-0.0071)	6.0871	(-0.0053)
200	22.3975	(-0.0463)	21.9807	(-0.0450)	7.7718	(-0.0048)	6.0838	(-0.0034)
Complex Kohn variational method, overset-grid expansion								
15/3	22.8492		22.4204		7.8700		6.0061	
25/3	22.0215	(-0.8277)	21.6151	(-0.8053)	7.7112	(-0.1589)	6.0572	(0.0511)
35/3	22.2841	(0.2626)	21.8705	(0.2553)	7.7574	(0.0462)	6.0760	(0.0188)

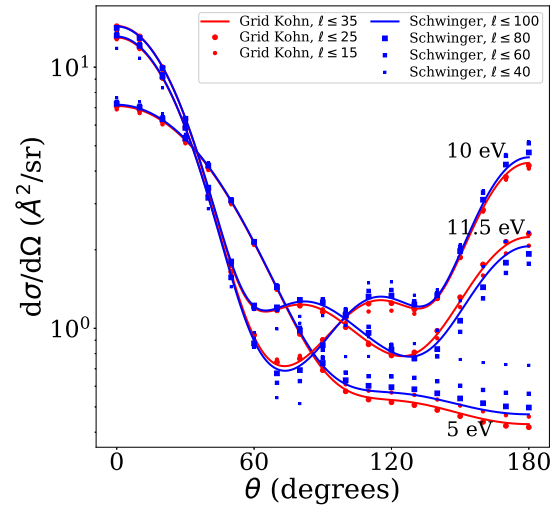


FIG. 9. Convergence of differential cross sections for CF_4 in the static-exchange approximation at 5 eV and at the energies of the centers of the resonance features: complex Kohn results, red dots and solid red line with the converged results at $\ell_{\max} = 35$; Schwinger results with single-center expansion, blue dots with solid blue line at $\ell_{\max} = 100$.

behavior of the methods at the T_2 resonance is similar, with the single-center expanded Schwinger method converging the magnitude of the resonance slowly from $\ell = 60$ to $\ell = 100$ and the grid Kohn method converging much more rapidly. For energies below 10 eV, the Schwinger T_2 cross sections also converge more slowly compared to the grid Kohn cross sections.

The convergence of the differential cross section is shown in Fig. 9, both at the resonance features and at 5 eV. As might be expected, the cross sections converge most slowly for backscattering and at the oscillations at intermediate angles for the resonance energies. In all cases the convergence of the grid-based complex Kohn results with added partial waves on the central grid is dramatically faster than the single-center expansion results.

In Table III we examine the convergence of the single-center and overset-grid expansions for the following points of interest: the A_1 components of the cross section at the very low energies (i) 0.01 and (ii) 0.1 eV, for which the potential near the nuclei must be well resolved, (iii) the center of the A_1 resonance feature at 11.5 eV, and (iv) the center of the T_2 resonance at 10.0 eV. For the A_1 and T_2 resonance cross sections, the Schwinger method converges to the values 7.8 and 6.1 \AA^2 by $\ell = 120$, respectively, and converges to 7.77 and 6.08 \AA^2 , respectively, with a tolerance of 0.005 \AA^2 by $\ell = 200$. At $\ell = 35$ for the central grid and $\ell = 3$ for the subgrid, the overset-grid Kohn method predicts cross sections for these resonances of 7.76 and 6.08 \AA^2 , in near perfect agreement with the Schwinger results but with many fewer partial waves. All of these comparisons are done with the maximum value of the radial variable r on the grids, both equal to 5.3 \AA , chosen purely for convenience to be just beyond the range of the exchange potential. Nonetheless, at the lowest energies the cross sections from the Schwinger and Kohn calculations agree only to within 0.1 \AA^2 , suggesting that the remaining small differences between them are due to slower convergence with respect to partial waves at low energies of the A_1 component of the T matrix seen in the table.

IV. SUMMARY

We have formulated an overset-grid version of the complex Kohn variational approach to electron–polyatomic-molecule collisions and demonstrated that it is a robust method for solving the scattering problem. The key components developed here, all necessary for this formulation, are an overcomplete (in principle) underlying spectral basis defined on overlapping subgrids and a central grid, simultaneous expansion of the scattering trial wave function in spherical harmonics about multiple centers, expansion of the trial function in the basis $\phi_k^+ = (\hat{G}_0^+ \hat{V})^k \phi_0$ in which all the basis functions satisfy outgoing-wave boundary conditions, and accurate operation of the free-particle Green’s function and exchange operators based on Gauss-Lobatto quadratures adapted for integration over subintervals required by the slope discontinuity in the radial Green’s function. This grid-based method will allow the application of the Kohn variational approach to both larger systems and higher energies and also removes the separable exchange approximation made in the previous implementation of the complex Kohn method for electron-molecule scattering.

Although in principle the spectral basis in the subgrids and central grid can become linearly dependent if the radial grids are made arbitrarily dense and the number of partial waves is greatly increased, two factors seem to minimize any effects of over completeness. First, the switching functions remove parts of the central grid that would overlap the majority of each subgrid volume and thus restrict potential problems

only to the overlapping annular volumes where the switching between grids occurs. Second, in this method the Born–Arnoldi iterative solution generates a small basis of functions on the grid that allows solution of the linear equations for the scattered wave function before any numerical pathologies due to potential linear dependence of the central grid and subgrid representations appears.

Toffoli *et al.* [54] have described and extensively applied a method for solving scattering problems using a density-functional theory that is based on overlapping, multicenter B -spline basis sets, in which a similar question arises. That method does not have the drawbacks of single-center expansions, but still manages to avoid numerical difficulties due to linear dependence even though it does not make use of switching functions like those used here. Those authors make an important observation that in their method the problem diminishes for atoms located far from the expansion center, precisely those for which the addition of the subgrids is most important. The same is true here, and the potential overcompleteness of the underlying spectral basis from the union of the subgrids and central grid has thus far produced no noticeable numerical pathologies.

While the principal motivation to represent the trial wave function of the Kohn approach on overset grids is to gain the accuracy and generality of grid representation in this variational approximation to the scattering amplitudes, the basis we have chosen in order to apply outgoing-wave boundary conditions produces a formal property for this approach not previously exploited in any implementation of Kohn’s original idea. In the present method a Padé approximant to the full solution of the scattering problem is being automatically constructed. That property allows the convergence of the T matrix with a basis of 20–30 functions defined by $(\hat{G}_0^+ \hat{V})^k \phi_0$ even for the largest grids used in these calculations.

This aspect of the method will be critical to the extension of this approach to multichannel calculations. All of the fundamental components necessary for implementing the close-coupling version of the complex Kohn method [1] have been demonstrated here. That extension to multiple scattering channels and the application of Coulomb boundary conditions within this framework are left to future work.

ACKNOWLEDGMENTS

Work at the University of California, Davis was supported by the US Army Research Laboratory and the US Army Research Office under Grant No. W911NF-14-1-0383. Calculations presented here made use of the resources of the National Energy Research Scientific Computing Center, a DOE Office of Science User Facility. Computational resources were also provided by Texas A&M High Performance Research Computing. Work performed at Texas A&M University was supported by the US Department of Energy, Office of Science, Basic Energy Sciences, under Award No. DE-SC0012198.

- [1] C. W. McCurdy and T. N. Rescigno, *Phys. Rev. A* **39**, 4487 (1989).
 [2] B. H. Lengsfeld, T. N. Rescigno, and C. W. McCurdy, *Phys. Rev. A* **44**, 4296 (1991).

- [3] S. D. Parker, C. W. McCurdy, T. N. Rescigno, and B. H. Lengsfeld, *Phys. Rev. A* **43**, 3514 (1991).
 [4] B. H. Lengsfeld and T. N. Rescigno, *Phys. Rev. A* **44**, 2913 (1991).

- [5] T. N. Rescigno, B. H. Lengsfeld III, and C. W. McCurdy, in *Modern Electronic Structure Theory*, edited by D. R. Yarkony (World Scientific, Singapore, 1995), Vol. 2, pp. 501–588.
- [6] T. N. Rescigno, C. W. McCurdy, A. E. Orel, and B. H. Lengsfeld III, *Computational Methods for Electron-Molecule Collisions* (Springer, Berlin, 1995), pp. 1–44.
- [7] C. S. Trevisan, C. W. McCurdy, and T. N. Rescigno, *J. Phys. B* **45**, 194002 (2012).
- [8] N. Douguet, D. S. Slaughter, H. Adaniya, A. Belkacem, A. E. Orel, and T. N. Rescigno, *Phys. Chem. Chem. Phys.* **17**, 25621 (2015).
- [9] R. R. Lucchese and V. McKoy, *Phys. Rev. A* **24**, 770 (1981).
- [10] R. R. Lucchese, G. Raseev, and V. McKoy, *Phys. Rev. A* **25**, 2572 (1982).
- [11] J. Tennyson, *Phys. Rep.* **491**, 29 (2010).
- [12] S. R. Leone, C. W. McCurdy, J. Burgdörfer, L. S. Cederbaum, Z. Chang, N. Dudovich, J. Feist, C. H. Greene, M. Ivanov, R. Kienberger *et al.*, *Nat. Photon.* **8**, 162 (2014).
- [13] F. Calegari, D. Ayuso, A. Trabattoni, L. Belshaw, S. De Camillis, S. Anumula, F. Frassetto, L. Poletto, A. Palacios, P. Decleva *et al.*, *Science* **346**, 336 (2014).
- [14] D. S. Slaughter, A. Belkacem, C. W. McCurdy, T. N. Rescigno, and D. J. Haxton, *J. Phys. B* **49**, 222001 (2016).
- [15] F. H. Ómarsson, E. Szymańska, N. J. Mason, E. Krishnakumar, and O. Ingólfsson, *Eur. Phys. J. D* **68**, 101 (2014).
- [16] T. N. Rescigno, C. S. Trevisan, A. E. Orel, D. S. Slaughter, H. Adaniya, A. Belkacem, M. Weyland, A. Dorn, and C. W. McCurdy, *Phys. Rev. A* **93**, 052704 (2016).
- [17] D. J. Haxton, H. Adaniya, D. S. Slaughter, B. Rudek, T. Osipov, T. Weber, T. N. Rescigno, C. W. McCurdy, and A. Belkacem, *Phys. Rev. A* **84**, 030701(R) (2011).
- [18] Y. Kawarai, T. Weber, Y. Azuma, C. Winstead, V. McKoy, A. Belkacem, and D. S. Slaughter, *J. Phys. Chem. Lett.* **5**, 3854 (2014).
- [19] C. Winstead and V. McKoy, *Radiat. Phys. Chem.* **77**, 1258 (2008).
- [20] A. Dora, J. Tennyson, L. Bryjko, and T. van Mourik, *J. Chem. Phys.* **130**, 164307 (2009).
- [21] W. Kohn, *Phys. Rev.* **74**, 1763 (1948).
- [22] N. Suhs, S. Rogers, and W. Dietz, *32nd AIAA Fluid Dynamics Conference and Exhibit* (AIAA, Reston, 2002), p. 3186.
- [23] R. L. Meakin, *Handbook of Grid Generation* (CRC, Boca Raton, 1998).
- [24] N. A. Petersson, *SIAM J. Sci. Comput.* **21**, 646 (1999).
- [25] W. Chan, R. Gomez, S. Rogers, and P. Buning, *32nd AIAA Fluid Dynamics Conference and Exhibit* (Ref. [22]), p. 3191.
- [26] A. D. Becke, *J. Chem. Phys.* **88**, 2547 (1988).
- [27] C. W. McCurdy, T. N. Rescigno, and B. I. Schneider, *Phys. Rev. A* **36**, 2061 (1987).
- [28] W. H. Miller and B. M. D. D. Jansen op de Haar, *J. Chem. Phys.* **86**, 6213 (1987).
- [29] J. Nuttall, *Phys. Rev.* **157**, 1312 (1967).
- [30] C. R. Garibotti, *Ann. Phys. (NY)* **71**, 486 (1972).
- [31] R. R. Lucchese and V. McKoy, *Phys. Rev. A* **28**, 1382 (1983).
- [32] A. E. Orel, T. N. Rescigno, and B. H. Lengsfeld, *Phys. Rev. A* **44**, 4328 (1991).
- [33] T. N. Rescigno, B. H. Lengsfeld III, and A. E. Orel, *J. Chem. Phys.* **99**, 5097 (1993).
- [34] A. Menssen, C. S. Trevisan, M. S. Schöffler, T. Jahnke, I. Bocharova, F. Sturm, N. Gehrken, B. Gaire, H. Gassert, S. Zeller *et al.*, *J. Phys. B* **49**, 055203 (2016).
- [35] C. W. McCurdy, T. N. Rescigno, C. S. Trevisan, R. R. Lucchese, B. Gaire, A. Menssen, M. S. Schöffler, A. Gatton, J. Neff, P. M. Stammer *et al.*, *Phys. Rev. A* **95**, 011401(R) (2017).
- [36] J. Lill, G. Parker, and J. Light, *Chem. Phys. Lett.* **89**, 483 (1982).
- [37] T. N. Rescigno and C. W. McCurdy, *Phys. Rev. A* **62**, 032706 (2000).
- [38] L. Tao, C. W. McCurdy, and T. N. Rescigno, *Phys. Rev. A* **79**, 012719 (2009).
- [39] R. R. Lucchese, *J. Chem. Phys.* **92**, 4203 (1990).
- [40] F. A. Gianturco, R. R. Lucchese, and N. Sanna, *J. Chem. Phys.* **100**, 6464 (1994).
- [41] J. P. Boyd, *Chebyshev and Fourier Spectral Methods* (Courier, North Chelmsford, 2001).
- [42] B. Basden and R. R. Lucchese, *J. Comput. Phys.* **77**, 524 (1988).
- [43] E. F. Valeev, LIBINT: A library for the evaluation of molecular integrals of many-body operators over Gaussian functions, version 2.1.0, 2014, <http://libint.valeev.net/>.
- [44] A. P. P. Natalense and R. R. Lucchese, *J. Chem. Phys.* **111**, 5344 (1999).
- [45] H.-J. Werner, P. J. Knowles, G. Knizia, F. R. Manby, and M. Schütz, *Wires Comput. Mol. Sci.* **2**, 242 (2012).
- [46] H.-J. Werner, P. J. Knowles, G. Knizia, F. R. Manby, M. Schütz, P. Celani, T. Korona, R. Lindh, A. Mitrushenkov, G. Rauhut *et al.*, MOLPRO: A package of *ab initio* programs, version 2012.1, <http://www.molpro.net>.
- [47] M. J. Frisch, G. W. Trucks, H. B. Schlegel, G. E. Scuseria, M. A. Robb, J. R. Cheeseman, J. A. Montgomery, Jr., T. Vreven, K. N. Kudin, J. C. Burant *et al.*, GAUSSIAN 03, revision C.02 (Gaussian, Inc., Wallingford, 2004).
- [48] T. Noro and H. S. Taylor, *J. Phys. B* **13**, L377 (1980).
- [49] W. J. Hehre, R. F. Stewart, and J. A. Pople, *J. Chem. Phys.* **51**, 2657 (1969).
- [50] J. B. Collins, P. von R. Schleyer, J. S. Binkley, and J. A. Pople, *J. Chem. Phys.* **64**, 5142 (1976).
- [51] W. J. Hehre, R. Ditchfield, and J. A. Pople, *J. Chem. Phys.* **56**, 2257 (1972).
- [52] P. C. Hariharan and J. A. Pople, *Theoret. Chim. Acta* **28**, 213 (1973).
- [53] M. M. Francl, W. J. Pietro, W. J. Hehre, J. S. Binkley, M. S. Gordon, D. J. DeFrees, and J. A. Pople, *J. Chem. Phys.* **77**, 3654 (1982).
- [54] D. Toffoli, M. Stener, G. Fronzoni, and P. Decleva, *Chem. Phys.* **276**, 25 (2002).